All-optical switch based on novel physics effects

Huixin Qi[1], Xiaoxiao Wang[1], Xiaoyong Hu[1,2,3,*], Zhuochen Du[1], Jiayu Yang[1], Zixuan Yu[1], Shaoqi Ding[1], and Qihuang Gong[1,2,3]

[1]*State Key Laboratory for Mesoscopic Physics & Department of Physics, Collaborative Innovation Center of Quantum Matter & Frontiers Science Center for Nano-optoelectronics, Peking University, Beijing 100871, China*

[2]*Peking University Yangtze Delta Institute of Optoelectronics, Nantong, Jiangsu 226010, China*

[3]*Collaborative Innovation Center of Extreme Optics, Shanxi University, Taiyuan, Shanxi 030006, China*

[*]Corresponding authors: xiaoyonghu@ pku.edu.cn

Huixin Qi and Xiaoxiao Wang contributed equally to this work.

Abstract

All-optical switches are one of the most important parts of integrated photonics. Ultra-high-speed and ultra-low energy consumption are two necessary indexes of all-optical switches. Traditionally, all-optical switches are designed based on micro-ring resonator, surface plasmon polaritons, photonic crystal, and metamaterial, etc. However, such platforms cannot satisfy the demand for high performance of all-optical switches. Recently, to break through the limitation of response time and energy consumption, some studies on novel physics appear, which contain PT symmetry and exceptional points, topological insulators and bound states in the continuum, etc. The application of new physical effects not only provides new research ideas for the all-optical switch but also broadens the design channel, which is expected to achieve ultra-compact, ultra-fast, and large-capacity all-optical information processing.

1 Introduction

At present, the explosive growth of global data has put forward an increasing demands on information processing technology for ultra-large data transmission capacity and ultra-high information processing rates [1]. With the continuous development of ultra-high-speed electronic integrated circuits, researchers consider using photons as information carriers to achieve ultrafast and ultra-low energy consumption photons integrated circuits [2-4]. All-optical switches with a high performance of on-chip, ultra-compact, high speed, and low power are highly desirable as essential building blocks in integrated photonics. An all-optical switch can be defined as a structure with a pump light controlling the ON/OFF transition of the signal light. Optical nonlinear material is an important part of the nanostructure, the change in the refractive index of which is dependent on the intensity of pump light, mainly use third-order nonlinear optical Kerr effect [5-7]. Because the ultrashort third-order nonlinear optical response to pump light and the large third-order nonlinear coefficient of the material, such switches can achieve

picosecond-femtosecond magnitude response time and lower energy consumption. The response time and energy consumption are the two main indexes of the optical switch. Classical schemes for all-optical switches based on photonic crystal, surface plasmons, micro-ring resonator, and metamaterials involve the dynamical control of the cavity resonance via a pump pulse [8]. Traditional all-optical switches are mainly based on traditional physics structures. Over the last decades, there has been significant progress in integrated optics in terms of decreasing response time and energy consumption. However, such structures cannot meet the requirements of high speed and large capacity information processing. Researchers introduce new physical structures based on these basic physical concepts to overcome these difficulties. Novel physics effects to realize all-optical switch have recently drawn broad attention from photonics communities because they offer higher speed and larger capacity information processing ability. PT Symmetry and exceptional points, topological insulators and bound states in the continuum in all-optical switch are new physical principle that becomes new research hot spot. In the review, we mainly introduce traditional concepts and realization methods of all-optical switch. Then detailly present novel physical means based on exceptional points, topological insulators and bound states in the continuum. Finally, compared with the traditional technology, we state the advantages of the new physical effect and looking forward to the future development trend.

2 Basic concepts and the development of significance performance indexes

2.1 Micro-ring resonator

The principle of the all-optical ultrafast switch based on the micro-ring is to change the coupling state between the waveguide and the micro-ring through the control light, to realize the controlling of the signal light output. It has been demonstrated that the switch control of signal light output can be realized by nonlinear material and pump light to change the resonant frequency of the micro-ring attribute to the refractive index variation of the nonlinear material. In 2007, Först et al.[9] utilized two waveguides and O^+-ion implantation covered micro-ring to make an all-optical ultrafast switch, which reaction time is 55 ps, shown in Fig. 1(a). In 2008, Waldow et al. [10]demonstrated a 25 ps-all-optical switch based on micro-ring, shown in Fig. 1(b). The nonlinear material is hydrogen silsesquioxane (HSQ), which is covered on the Si waveguide. In 2014, Pelc et al. [11]carried out an all-optical ultrafast switch taking advantage of hydrogenated amorphous silicon Micro-ring resonators, shown in Fig. 1(c). Investigators observed that the reaction time of the all-optical switch is up to 14.8 ps. The pump lights' pulse width is 2.7ps, corresponding to a pulse energy of 3.0 pJ. They also measured the reaction time of the crystalline Si (c-Si) micro-ring resonators all-optical switch, which turned out to be 308 ps , 21 times longer than a-Si:H.

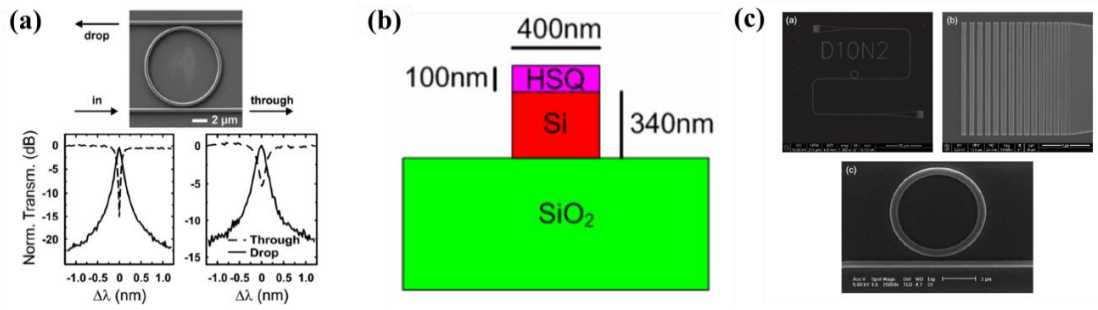

Fig. 1 Configuration characteristics of micro-ring devices. (a) Micrograph of the investigated micro-ring resonator after implantation. (b) Schematic cross sectional view of the SOI waveguide. (c)Scanning electron micrographs of a-Si: H devices after etching: layout of the micro-ring device with bus waveguide and grating couplers; close-up of the grating coupler for TM-polarized light; a 5-μm-diameter a-Si: H micro-ring and bus waveguide.

2.2 Surface plasmon polaritons

The surface plasmon polaritons (SPPs) based all-optical ultrafast switch has aroused people's concern in recent years. The basic idea is to affect the propagation characteristic of the SPPs, which can realize the change of optical path switch. One way to affect the propagation characteristic of the SPPs is using pump light. In 2019, Ono et al.[12] all-optical ultrafast switch, which switches energy is only 35 fJ and switches time reached 260 fs, shown in Fig. 2(a). They managed to couple the light from Si-waveguide into graphene-loaded deep-subwavelength plasmonic(Au) waveguides. This configuration promoted the absorption effect of the nonlinear material. In 2018, Zhang et al.[13]studied tunable plasmon-induced transparency(PIT) based multi-channel all-optical switch, which worked at telecommunication wavelengths, shown in Fig. 2(b). They covered the substrate with a silver layer, dug metal-insulator-metal (MIM) plasmonic waveguide, a stub resonator, and square ring resonators(SRRs). The stub resonator is used to couple the waveguide and SRRs. They filled the SRRs with nonlinear Kerr material or covered the SRRs with graphene layers. Both of these operations can help to realize an all-optical switch. The switch can work at multi wavelengths. Different polarization lights transformed differently in SPPS, which offered a potential method to realize SPPs based all-optical switch. In 2020, Karabchevsky et al.[14] utilized a different method to realize an SPPs based all-optical ultrafast switch, shown in Fig. 2(c). They demonstrated an all-optical sensor switch caused by the excitation of molecular overtones in a hybrid plasmonic-dielectric configuration. Their switch is controlled by the polarization state of the light, which is on when the incident light is TM wave, and off when it's TE wave.

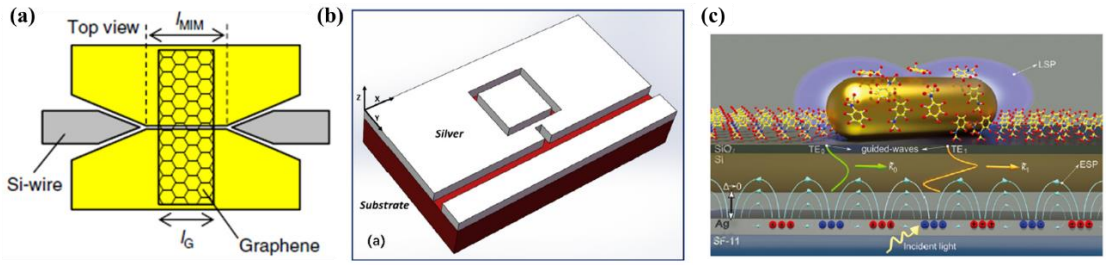

Fig. 2 Configuration characteristics of SPPs devices. (a) Top-view schematic of the graphene-loaded MIM-WG. (b) 3D schematic of structure with multilayer graphene. The relevant structure parameters: w = 100 nm, s = 123 nm, h = 190 nm, g = 15 nm, w' = 50 nm, L = 405 nm. (c) The coupling mechanism of the hybrid GWSPR-LSPR-overtone system (out of scale, the gap between the Ag and the Si layers is infinitesimally small with $\Delta \to 0$).

2.3 Photonic crystal

Photonic crystals(PCs) have pretty well wavelength selectivity. However, when the pump light is injected into the system, the transmission spectrum changes. For injected light in some wavelengths, the propagate state changes from allowing to forbidding or from forbidding to allowing, making it possible to make an all-optical switch. In 2016, Colman et al.[8] demonstrated a nanocavity-based photonic crystal all-optical switch shown in Fig. 3(a). They dug an input waveguide, an output waveguide, and a nanocavity in the photonic crystal. They found that the resonance wavelength of the cavity can be changed by both the kerr effect and free carriers and can realize all-optical switches, but the latter is better. Besides, they also proved the importance of coherent effects, which is always ignored when studying nanocavity dynamics. In 2017, Chai et al. [15]demonstrated an epsilon-near-zero (ENZ) nanocomposites-based ultrafast all-optical switch, which can be triggered remotely shown in Fig. 3(b). They dug two nanocavities and three silicon photonic crystal waveguides, two of which are used to couple the nanocavities to the signal transmission waveguide. The resonance wavelength of the nanocavities near 1560 nm. However, the two nanocavities coupled with each other caused the movement of the resonance wavelength, which means, Rabi splitting. Light at the wavelengths of 1559.8 nm and 1560.2 nm is banned, while light at the wavelengths of 1560nm can propagate. To activate the switch, the pump light with an intensity of 560 kW/cm^2 is injected to nanocavity A, causing its resonant wavelength to increase slightly. The effect is that the coupling effect between the nanocavities is greatly weakened, the Rabi splitting phenomenon disappears, and light at the wavelengths of 1560nm is forbidden. The all-optical switch has a response time of up to 15ps. In 2020, Takiguchi et al.[16] firstly demonstrated a picosecond all-optical switch utilizing a nanowire shown in Fig. 3(c). They put an InP/InAsP nanowire on a silicon photonic crystal. The line-defect photonic crystal has a Q-factor of 25000. Then, they found that the detuning(λ_pr-λ_c, λ_pr represent the probe laser wavelength while λ_c means cavity wavelength) was -0.25 nm, which contribute to the fastest reaction. The reaction time of the switch is 150ps, while the switching energy is several hundred fJ. The switch time and energy are both lower than the previously reported results.

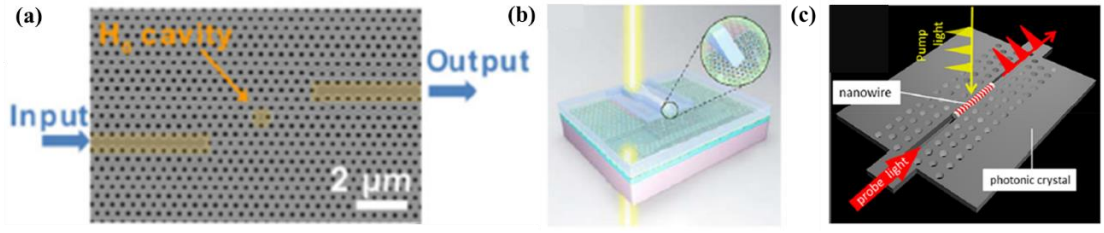

Fig. 3 Configuration characteristics of photonic crystal devices. (a) SEM image of the H_0 cavity and its access waveguides. (b) Structure schematic and scanning electron microscope (SEM) image

of the remotely-coupled photonic crystal nanocavities sample without the monolayer graphene, the nanocomposite nano-Au:(Er^{3+}:Al_2O_3) layer, and the uppermost Er^{3+}:Al_2O_3 waveguide. A and B indicate the photonic crystal nanocavities. I and O indicate the input- and output-coupling ports for the bus signal waveguide. (c) Schematic of a single-nanowire all-optical switch on a silicon PC.

2.4 Metamaterial

In 2020, Shoaei et al.[17] utilized nonlinear hyperbolic metamaterial to design an all-optical switch, which worked in visible and near-infrared regions, shown in Fig.4(a). They investigated three kinds of metamaterials. The first is Au-Al_2O_3 nanolayers. Switch using this nanolayer can be realized in the 585-600 nm range, and the transmittance of the 'on' state is from 52-72%. The pump signal they used is 500 V/μm. The second is Au/ Al_2O_3/G(graphene)/ Al_2O_3/Au nanolayers, corresponding work range is 803-805nm, 97% transmittance is reached, 4 V/μm pump signal. The last is Ag/Si/G/Si/Ag nanolayers, which can work over a wider wavelength range, 800-895 nm. The transmittance of the 'on' state is from 49-99%. The pump signal they used is 19.5 V/μm. In 2020, Xie et al.[17] designed an epsilon-near-zero(ENZ) metasurface-based optical switch, which can be controlled by electronic or optical, shown in Fig. 4(b). When using it as an all-optical switch, pump light incident on the metasurface with an angle(θ), motivating the nonlinear response of the ITO material at ENZ wavelength(1240nm). The transmission of the probe light can be tuned by both the θ and the pump light's intensity. The extinction ratio is over 5dB, and the reaction time is about 650fs.

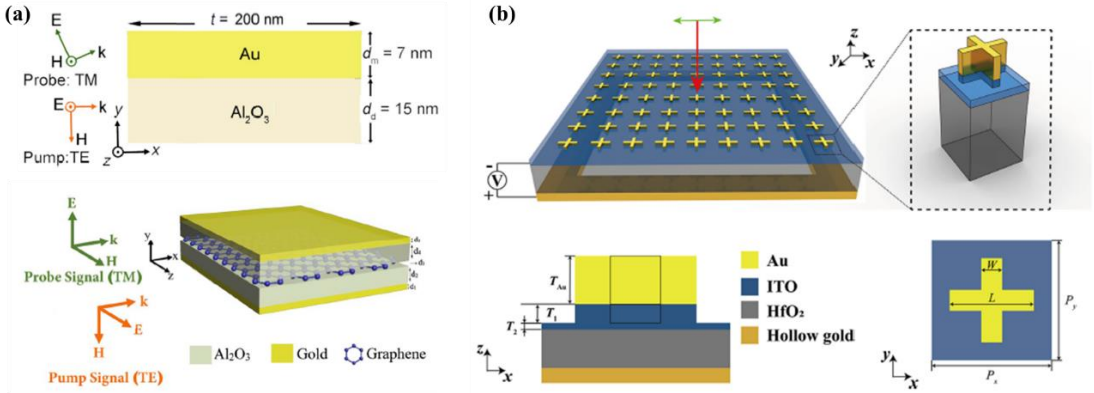

Fig. 4 Configuration characteristics of metamaterial devices. (a) Side (x–y plane) view of the unit cell of the HMM structure, composed of Au⁄Al_2O_3 nanolayers, under the illumination of a TE-polarized Gaussian pump and a TM-polarized CW probe. Unit cell of a switchable HMM, composed of Au/Al_2O_3/G/Al_2O_3/Au nanolayers, periodically repeated in the y-direction. Inset on the left depicts a TE-polarized pump signal and a TM-polarized probe signal. (b) 3D schematic overview of the proposed structure, with a cross-shaped array of Au and ITO located on top of an ITO nanofilm on the HfO_2 substrate. An x-polarized plane wave normally incident on the metasurface.

3 Novel physics effects to realize all-optical switch

3.1 PT Symmetry and exceptional points in all-optical switch

3.1.1 Non-Hermitian system and PT symmetry in optics

Concepts of the non-Hermitian system and Parity-Time(PT) symmetry firstly aroused in quantum field theory. For a physical system which is described by a Hamiltonian $\widehat{H}$, satisfying the equation $\widehat{H} = \widehat{H}^{\dagger}$ means the system is Hermitian with real energy eigenvalues and complete orthonormal eigenstates. However, if the Hamiltonian is not invariant under a Hermitian conjugate, the system is non-Hermitian. In general, a non-Hermitian system has open boundary conditions or just has gain or loss. Non-Hermitian systems can have imaginary energy eigenvalues unless the system has Parity-Time symmetry [18]. Considering a non-Hermitian Hamiltonian $\widehat{H} = \frac{\hat{p}^2}{2\mathrm{m}}$, if $\widehat{H}$ has PT symmetry which means $[\widehat{H}, \hat{P}\hat{T}] = 0$, the complex potential must satisfy $\mathrm{V(x)} = \mathrm{V}(-\mathrm{x})^*$.

In an optical system, concepts of the non-Hermitian system and PT symmetry are also widely discussed. Firstly, we start with the paraxial wave equation of diffraction used in optics in Eq. (1):

$$\mathrm{i}\frac{\partial \vec{E}(\mathrm{x},\mathrm{z})}{\partial \mathrm{z}} + \frac{1}{2\mathrm{k}}\frac{\partial^2 \vec{E}(\mathrm{x},\mathrm{z})}{\partial x^2} + \mathrm{k}_0\tilde{\mathrm{n}}(\mathrm{x})\vec{E}(\mathrm{x},\mathrm{z}) = 0 \tag{1}$$

where $\tilde{n}(x)$ is the complex refractive index distribution[19-21]. This equation is mathematically isomorphic to the Schrödinger equation, so we can establish the equivalence between quantum theory and light dynamics. Therefore, the effective Hamiltonian of the paraxial wave equation can be expressed as Eq. (2)

$$\widehat{H} = -\frac{1}{2k}\frac{\partial^2}{\partial x^2} - k_0\tilde{n}(x) \tag{2}$$

For a non-Hermitian PT-symmetric optical system, the complex refractive index distribution should satisfy $\tilde{n}(x) = \tilde{n}(-x)^*$.

An easier way to build a PT-symmetric optical system is to use the coupled mode equations[22] in Eq. (3).

$$\frac{\mathrm{d}}{\mathrm{d}\xi}\begin{pmatrix} a_1 \\ a_2 \end{pmatrix} = -\mathrm{i}\begin{pmatrix} \omega_1 - \mathrm{i}\gamma_1 & \kappa \\ \kappa & \omega_2 - \mathrm{i}\gamma_2 \end{pmatrix}\begin{pmatrix} a_1 \\ a_2 \end{pmatrix} \tag{3}$$

According to the coupled mode equations, to establish a PT-symmetric system, all we need are two coupled optical systems or just two coupled modes whose parameters satisfy particular conditions to make the eigenvalues real. We can freely use two coupled waveguides, two coupled cavities, or generally several waveguides and several resonators coupled with each other.

As an example, two coupled waveguides can form a PT-symmetric system with gain and loss [23,24]. As shown in Fig. 5, the two waveguides with constant coupling strength are fabricated from Fe-doped $LiNbO_3$. In this system, the gain is built up through two-wave mixing by selectively irradiating one of the waveguides with a pulsed laser. The other waveguide has a loss, which is from the optical excitation of electrons fromFe^{2+} centers to the conduction band.

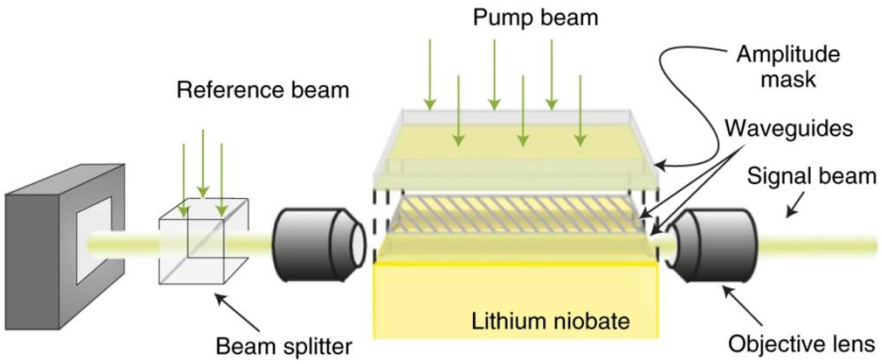

Fig.5 A PT-symmetric system consisting of two coupled waveguides: An Ar^+ laser beam (wavelength 514.5 nm) is coupled into the arms of the structure. An amplitude mask blocks the pump beam from getting into channel 2, enabling two-wave mixing gain only in channel 1.

Another kind of system does not have PT symmetry, such as a system that only has loss without gain. Nevertheless, gauge transformation can reveal the hidden PT symmetry and transfer the Hamiltonian to the one with PT symmetry. The properties of the PT symmetry remain in this kind of system, called passive PT symmetric system [25].

3.1.2 Fundamental of exceptional points

In a non-Hermitian PT symmetric system, there can be exceptional points(EPs) where the eigenvalue degenerates as well as the eigenstates. EPs are also called non-Hermitian exceptional points because they are quite different from the degenerate points(Dirac Points) in a Hermitian system. At DPs, the eigenvalue degenerates but the eigenstates are non-degenerate. However, at EPs, the eigenstates also degenerate, which means the eigenspace at EPs has a lower dimension.

Take two-dimensional coupled mode equations as an example. The effective Hamiltonian can be expressed as Eq. (4)

$$\begin{pmatrix} \omega_1 - \mathrm{i}\gamma_1 & \kappa \\ \kappa & \omega_2 - \mathrm{i}\gamma_2 \end{pmatrix} \tag{4}$$

We can derive the eigenvalues according to the Hamiltonian in Eq. (5):

$$\sigma_{\pm} = \omega_{ave} - \mathrm{i}\gamma_{ave} \pm \sqrt{\kappa^2 + \left(\omega_{diff} + \mathrm{i}\gamma_{diff}\right)^2} \tag{5}$$

where $\omega_{ave} = (\omega_1 + \omega_2)/2$ and $\gamma_{ave} = (\gamma_1 + \gamma_2)/2$ represents the mean values of the two subsystems' frequencies and loss factors, whereas $\omega_{diff} = (\omega_1 - \omega_2)/2$ and $\gamma_{diff} = (\gamma_1 - \gamma_2)/2$ are the differences between their frequencies and loss factors. If we assume the coupling strength κ, ω_{ave} and γ_{ave} are constant, we evaluate the evolution of real and imaginary parts of the eigenvalues in the parameter space $(\omega_{diff}, \gamma_{diff})$, in Fig. 6(a) and Fig. 6(b) [22]. Clearly, we can know that for a PT-symmetric system, the imaginary part of the eigenvalues vanishes, so there must be $\omega_{diff} = 0$, $\gamma_{ave} = 0$ and $\gamma_{diff} < \kappa$. The exceptional point is at $(0, \kappa)$in Fig. 6(a) and Fig. 6(b) and the parameters allowing PT-symmetric is on the one side of the EP.

If we change the coupling strength κ, the eigenvalues are evolutionary [23] as shown in Fig. 6(c) and Fig. 6(d). We can approach the EPs or break PT-symmetry by controlling the parameter in the system. And clearly, EPs are the critical points when breaking the PT symmetry.

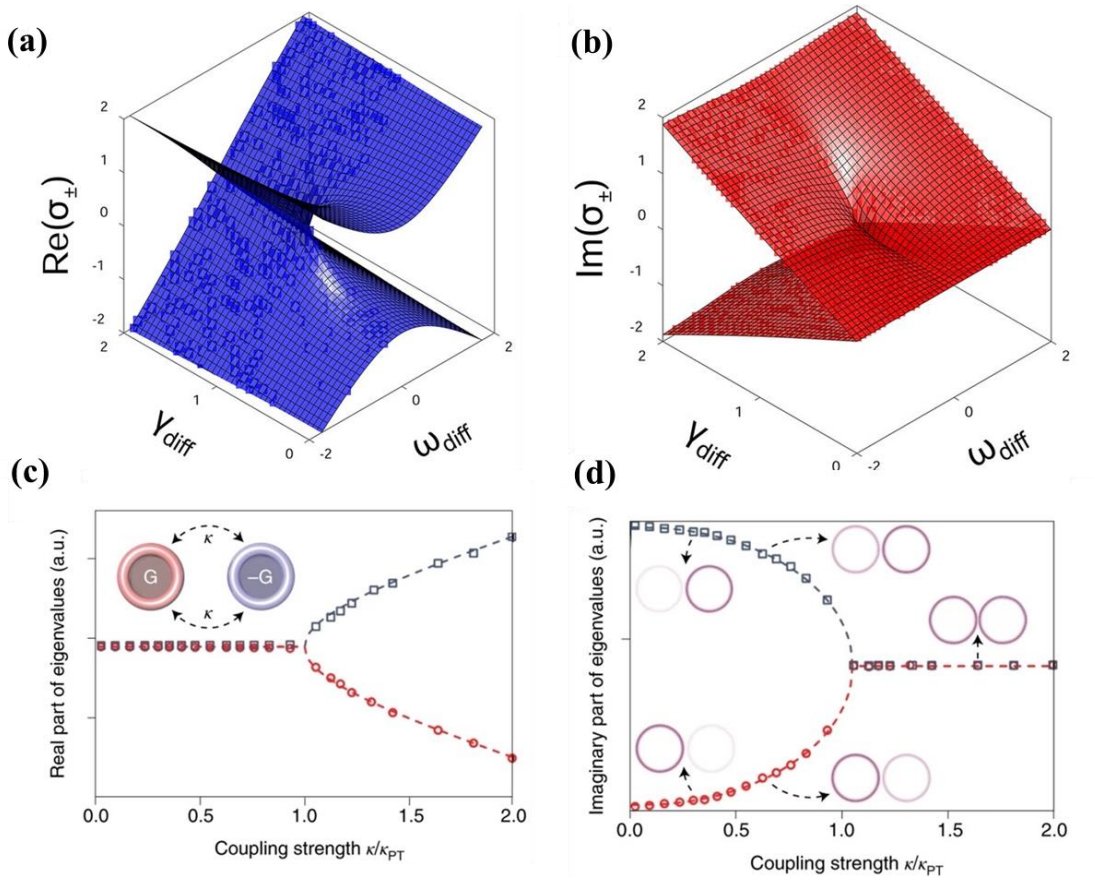

Fig.6 Evolution of eigenvalues while changing parameters of the system. (a)(b): Evolution of the real (A) and imaginary (B) parts of the eigenvalues of the system described by two-dimensional coupled mode equations in the two-dimensional parameter space $(\omega_{diff}, \gamma_{diff})$. Each diagram is a Reimann surface with two sheets. (c)(d): Evolution of the real (C) and imaginary (D) parts of the eigenvalues of the system when changing the coupling strength κ. Red circles and blue squares are obtained by numerical simulation in COMSOL assuming that the system is composed of resonators. κ is normalized to the critical coupling strength κ_{PT} at which the system approaches the EP.

3.1.3 Exceptional points applied to all-optical switch

EPs in the optical system have attached lots of attention in recent years. Researches on EPs are focused on EP encircling and the enhancement effects around EPs. For all-optical Switch, encircling EPs is a remarkable way.

Theoretically, when controlling two parameters of the system and others remain constant, the eigenvalue will evolve along a particular path on the Riemann surface in the space of parameters, like $(\omega_{diff}, \gamma_{diff})$ in Fig. 6(a) and Fig. 6(b). When changing the parameters sufficiently slowly, as well as continuously encircling an EP, an adiabatic state evolution will come up. As shown in Fig. 7(a) and Fig. 7(b), the endpoint of the path and the mode switches are possibly on a different Riemann sheet while encircling the EP. Which Riemann sheet the endpoint will be on only depends on whether the loop is clockwise(CW) or counter-clockwise(CCW)[26].

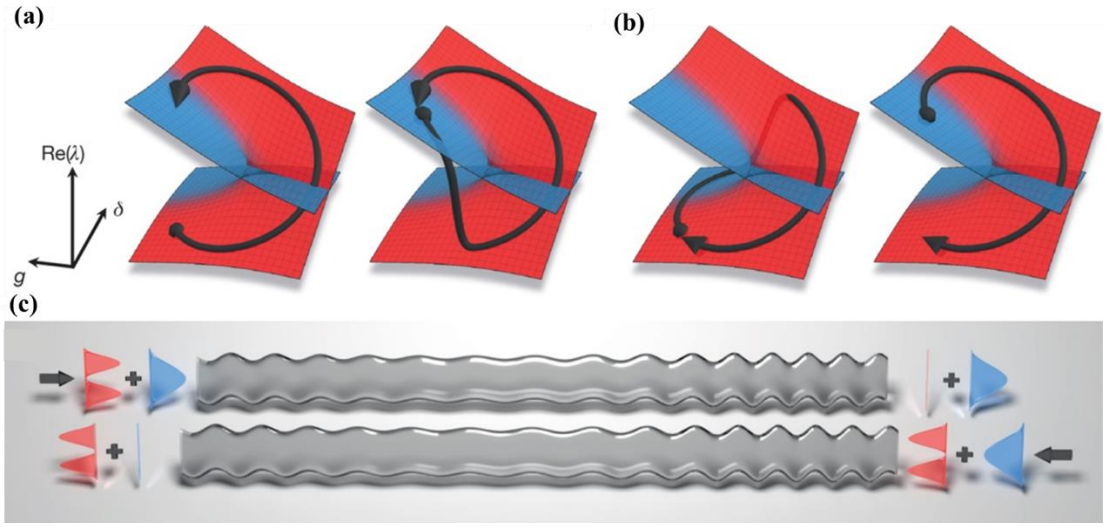

Fig.7: Mode switch when encircling EP. (a)(b): Encircling EP counter-clockwise(a) or clockwise(b), then the endpoint will always be on the blue(a) or red(b) Reimann sheet, which means transfer to an odd mode or even mode respectively. (c): Two-mode waveguide designed to perform an EP-encircling while propagating through it. Injection from the right or left accomplishes the EP-encircling clockwise or counter-clockwise respectively.

For example, in 2016, J. Doppler and the co-workers applied the theory of encircling an EP to a two-mode waveguide and proved the theory experimentally [26]. Eigenstates of the effective Hamiltonian are the even and odd modes in this waveguide. Controlling of the two parameters(g denotes the coupling and δ denotes detuning) is implemented by a smooth variation of the modulation potential of the waveguide. As shown in Fig. 7(c), EP-encircling is achieved when propagating through the designed waveguide and only one of the two transverse modes will get through the waveguide depending on the injection direction. Right, and left injection corresponds with CW loop and CCW loop respectively.

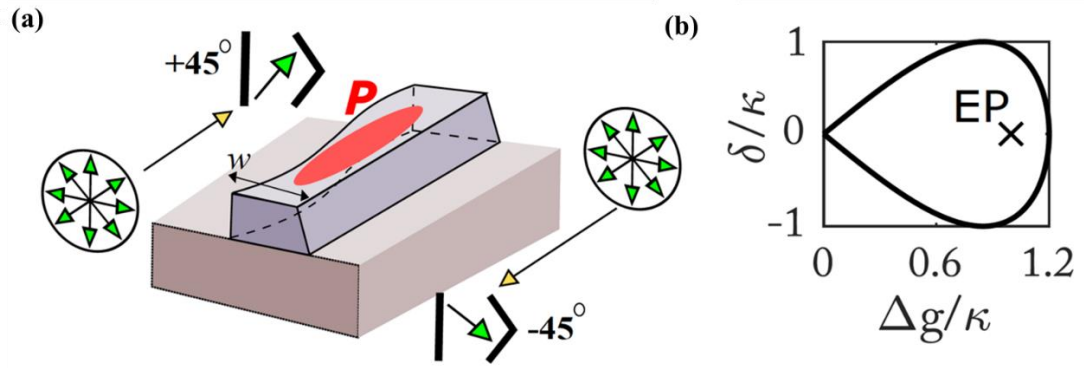

Fig.8 The designed waveguide to achieve polarization modes switch: (a) The waveguide with variations in the width(w) sinusoidally and pumping(P) which is strongest in the center. The eigenstate of the system is shown by green arrow-heads. (b) EP-encircling in the parameters space for this system. Detuning is given by δ and Δg represents the difference between the TE and TM modal gains.

Similarly, in 2017, A. U. Hassan and co-workers theoretically proved the EP-encircling theory by solving the differential equation mathematically [23]. They re-casted the coupled mode equations into two re-casted into a second-order differential equation while two parameters are encircling EP and depend on only one parameter, which can be reduced to the form of degenerate hypergeometric differential equations. Then by showing the asymptotic expansion when encircling slowly enough they proved the mode switch after the encircling. They applied the theory to a waveguide which is the right trapezoid shown in Fig. 8(a) as well as the eigenstates. The variations in the width and pumping of the waveguide can achieve EP-encircling in Fig. 8(b). No matter what direction of the polarization state injects the waveguide, the output will only be particularly one of the eigenstates in Fig. 8(a) depending on the whether the CW or the CCW loop the design of this waveguide makes.

Second-order EPs which means two eigenvalues and eigenmodes degenerate are now widely used to achieve all-optical switch. Higher-order EPs are also achieved [25]. People have different ways to design an optical system and approach the EPs, then they find ways to encircling the EPs and achieve a mode switch. The EPs are getting more and more attention in recent years.

3.2 Topological insulators in all-optical switch

3.2.1 The introduction of topological insulators

The initial idea of topological insulators arouses from condensed matter physics, paying attention to electrons moving along the surface of some specially designed materials. in brief, topological insulators are materials that behave as insulators in their interior but are conductive on their surfaces [27].

Topological insulators are well-studied because of their good properties and promising applications. The most well-known property is that traditional topological insulators allow electrons to propagate along the boundary, neglecting the defects and will not dissipate even if there are corners or turnings. It can be used in the fabrication of low-loss waveguides when we are talking about photonic topological insulators. Also, non-trivial topological insulators allow gas of helical Dirac fermions that behave like massless relativistic fermions. Besides, Spin-momentum locking is observed in topological insulators, which can be used to invent spintronic devices.

Photonic topological insulators are just like topological insulators but the relevant particle is photons rather than electrons . The theories of photonic topological insulators are mostly the same as those of electronic topological insulators. They can provide robust unidirectional channels for light propagation, as expected.

Due to the special properties of topological insulators, these applications mentioned before are quite promising to have more advantages than traditional designs. There are a variety of models of topological insulators owing to the different ways to fulfill the topological properties.

3.2.2 The application of topological insulators in all-optical switch

Valley photonic crystals, for example, are prospective materials to realize topological optical switches with some vital advantages. In 2018, Wu et al. [28] theoretically put

forward a design of topological optical switches while studying reconfigurable topological states in valley photonic crystals, as shown in Fig. 9. They simply construct two topologically distinct valley photonic crystals to form a two-port optical switch. By tuning the refractive index of one rod in each unit cell, the inversion symmetry is broken, leading to nontrivial topology locked to each valley. ω = 0.3678a/2πc is chosen for a working frequency, where D > 92% for both ports. The ON/OFF ratio is 32.8(28.9) for the left (right) port. In conclusion, the two-port optical switch put forward here not only has good performance but can also tolerate some defects or impurities due to the topological protection.

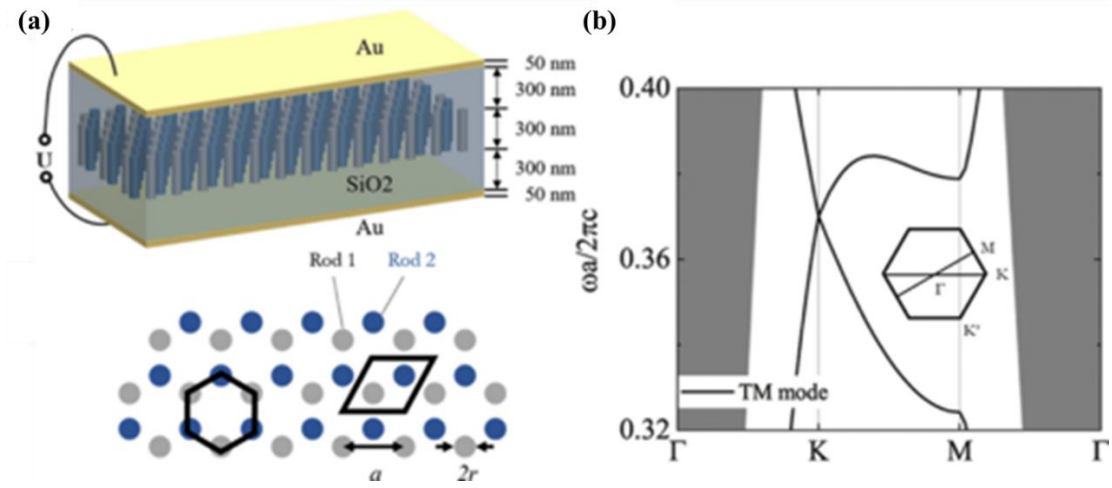

Fig.9 (a)Three-dimensional configuration of the reconfigurable valley photonic crystal. The photonic crystal rod slab is embedded in a SiO2 layer and covered by two gold films. The band structure of the TM mode for the two-dimensional photonic crystals when $n_{\mathrm{TiO2}} = n_{\mathrm{BTO}}$. (b) Schematic of a two-dimensional model of the valley photonic crystal composed of TiO2 (rod 1, gray rods) and $BaTiO_3$ (rod 2, blue rods).

Low-dimensional topological insulator Bi_2Se_3, a state-of-the-art quantum phase epitomized by the insulating bulk band gap and metallic surface states. Utilizing the polarization-sensitive characteristic of the non-linear absorption effect inside the Bi_2Se_3-Au nanoantenna hybrid-structure, as shown in Fig.10, Miao et al. in 2019 [29] designed a kind of optical switch which can be easily modulated by simply rotating the light polarization with a right angle. The polarization-sensitive characteristic of the non-linear absorption effect comes from the localized surface plasmon resonance of the used topological insulator, Bi2Se3-Au. The superiority of this design is that it can be used in purely optical systems without introducing complex structures. Also, it can be easily manipulated. Through a light-control-light system, the transmittance intensity of 450 nm and 1064 nm continuous-wave probe light can be modulated by the 800 nm fs-laser pump light (~10 GW cm^{-2}). Thus, the "ON" and "OFF" modes induced by the intensity of the probe light with the structure-based switch are achieved.

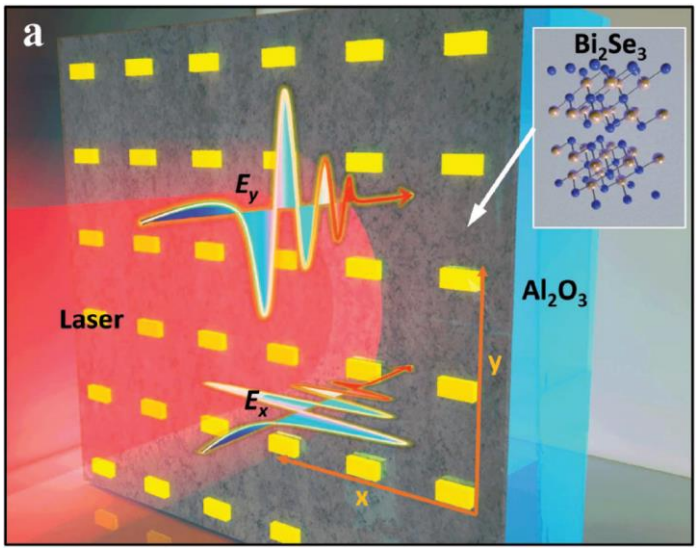

Fig.10 A schematic diagram of the Bi_2Se_3-Au nanoantenna hybrid-structure sample on an Al_2O_3 substrate under laser irradiation

In 2020, Lin et al. [30] present a tunable light absorption of graphene using topological interface states. The monolayer graphene is embedded in the interface of asymmetric topological photonic crystals, which can be shown in Fig 11. Topological interface states excite a strong absorption phenomenon whose intensity is sensitively related to the chemical potential of graphene and the periodic number of the asymmetric topological photonic crystals. As a result, as long as the chemical potential slightly varies in value, near 1.2 eV, the absorption displays a quick attenuation in a tiny region, which is a benefit to the application of optical switch and others.

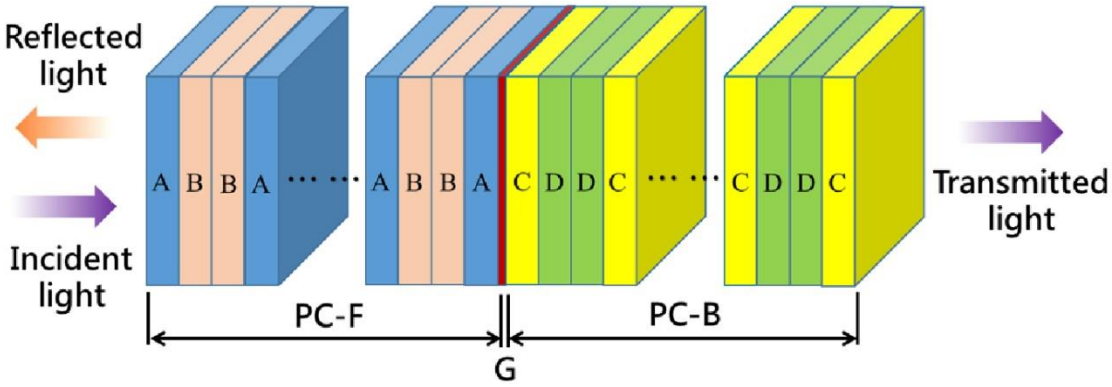

Fig.11 Schematic diagram of the one-dimensional asymmetric topological photonic crystals with graphene.

3.3.Bound states in the continuum in all-optical switch

3.3.1 Fundamental concept of bound states in the continuum

Bound states in the continuum (BICs) are waves that are spatially localized in the case where they coexist with continuous radiation waves that can carry energy away. It represents a general wave phenomenon observed in photonics, acoustic, elastic waves, which were originally proposed by von Neumann and Wigner in custom-constructed

potentials in an electronic system.

Generally, in an open system, the frequency spectrum consists of a continuous spectrum of one or more extended states that capable of propagating energy outward and several discrete bound states resulting from multiple potential wells. There are several different mode profiles, the mode profile lying in discrete levels of conventional bound states (green line in Figure.12) is the regular bound state which is confined in a structure or potential. (black dashed line in Figure.12) It has no channel to carry outgoing flux and couple with the outer environment because it doesn't have enough energy on its own to climb out of the confinement well. The ordinary mode profiles that exist across a continuous range of frequencies are extended states (blue line in Figure.12) that can propagate energy outward. The leaky mode appears in the continuum that is capable of coupling to the extended waves and leaks out, it is the resonance (orange line in Figure.12) that can be expressed with a complex frequency, $\omega = \omega_0 - i\gamma, \omega_0$ is the resonance frequency and the γ is the leakage rate. Bound state in the continuum (BIC) (red line in Figure.12) is an exception to the conventional cases mentioned above. Although it resides within the spectral continuum of propagating waves that radiate to the far-field, BICs decouple completely from the extended waves, so it remains perfectly confined without any radiation. A BIC is always considered as a resonance without leakage($\gamma = 0$), in other words, a BIC has zero linewidth and infinite quality factor($Q = \omega_0/2\gamma$) [31,32].

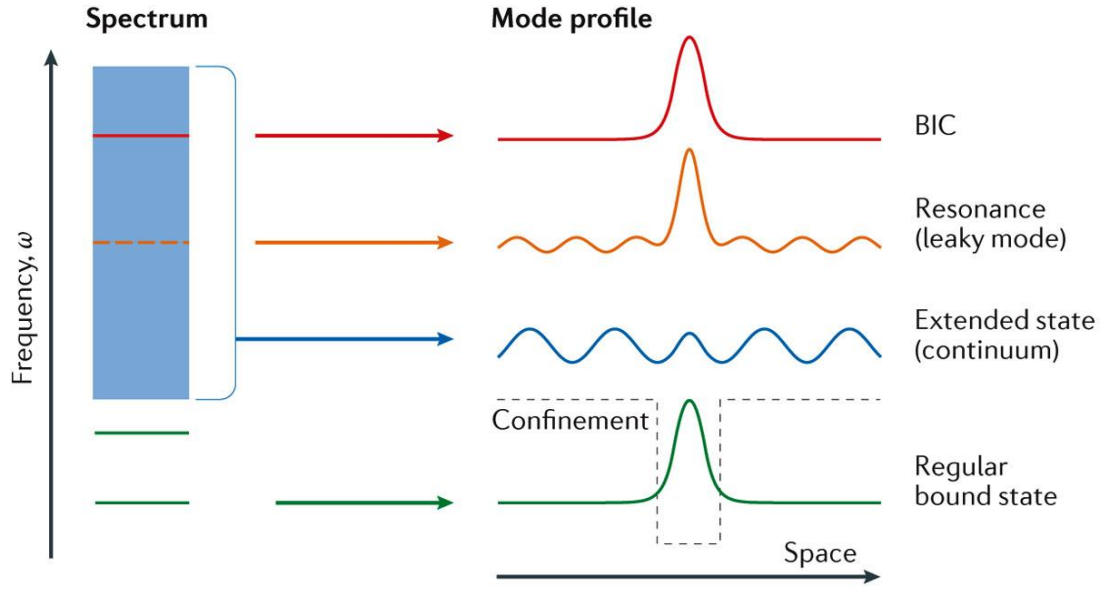

Figure.12 Explanation of a BIC. Spectrum: the frequency spectrum consists of a continuum or several continua of spatially extended states (blue) and discrete levels of bound states (green) that carry no outgoing flux in an open system. Mode profile: Bound states in the continuum (BICs; red) are exceptional states that lie inside the continuum but remain localized without radiation. Leaky modes lie in the continuous spectrum typically couple to the extended waves and radiate, becoming leaky resonances with resonance frequency has imaginary part (orange). Spatially extended states (blue). Discrete levels of bound states (green).

Various mechanisms have been proposed to create BICs. It's concluded that the

important concept to produce BICs is decoupling. For periodic systems, they can be classified into two types: symmetry-protected BICs and Parameter tuning BICs [33]. The symmetry-protected BICs appear when the spatial symmetry of the model is different from the symmetry of the radiative wave propagating energy outward, the coupling between the environment and modes is forbidden. Parameter tuning BICs appear when completely suppressing radiation into all channels through tuning the parameters of the system. BICs and quasi-BICs are generally used in the application, such as lasing, sensing, and filtering. BICs have an infinite quality factor in an ideal case with no radiation, it can't be excited by waves coming from the far field. Quasi-BICs break the symmetry of the structure with a finite quality factor, it can not only be excited by the outside field but also can radiate out.

3.3.2 Some examples about the bound states in the continuum in all-optical switch

Quasi-BICs are always used to generate high Q resonances which are important to enhance light-matter interaction. The result of the high Q resonances is the sharp spectral resonance that is of great importance to many applications such as optical switch [34], imaging [35], filtering [36].

In 2019, Karl et al. [37] explored a structure of the dielectric metasurface based on symmetry broken with a $230 \times 80\, nm^2$ part removed from one corner of a $300 \times 300\, nm^2$ resonant structures, as shown in Fig. 13(a). The structures are arranged in a square array , and the lattice constant is 470 nm. A Fano resonance appear at 970 nm resulting from interaction between the in-plane ED and an out-of-plane MD, it's can be observed from the reflectance spectrum. A spectral shift is achieved with lower pump fluences ($89\ \mu J/cm^2$) compared to the previous, and with short recovery times (2.5 ps), which could be applied to optical switch. In 2020, Zhong et al. [38] provide a configuration where a continuous graphene monolayer is placed between the dielectric grating and distributed Bragg reflector (DBR) layers, as Fig. 13(b) schematically depicted. This system effectively suppresses both the external leakage loss rate and intrinsic absorption loss rate. with the increase of the distance (hs) between graphene and DBR, the linewidth of the resonances disappears and the Q factor increases quickly(up to 50833), indicating that BICs appear. They further achieve high performance switch manipulation by introducing nonlinear dielectric. The switch is controlled from "off" to "on" with just 0.2 eV chemical potential or $5\ \mathrm{kW/cm^2}$ pump light, and the absorption contrast ratio reaches 31 dB. In 2021, Han et al. [39] exploit a slotted silicon disk array which shows the high Q resonances based on the BIC phenomenon, besides come up with a device of all-optical self-switch. The unit cell and band structure can be shown in figure 3. The BIC mode has no interaction with external environment, because all its radiative channels are closed. The air slot plays an important role in the transition from the BIC mode to Quasi-BIC mode. The laser power intensity level of all-optical self-switch less than $1\mathrm{kW}/cm^2$ is required to achieve a change of transmittance from 0 to above 65%.

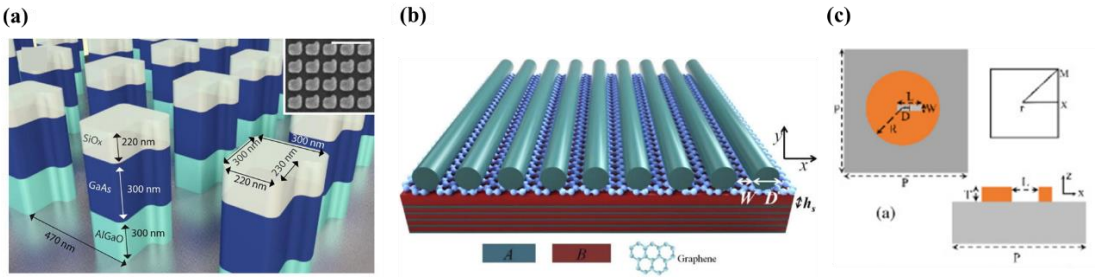

Figure.13 (a)Illustration of the dielectric metasurface. The geometry of the three-layer symmetry broken structure with GaAs sandwiched by low index materials. The inset is the SEM image of the fabricated device. (b)Schematic of the structure of the ultra-high Q graphene perfect absorber. (c) Schematic of the unit cell of slotted silicon disk array structure.

4 Discussion and outlook

In conclusion, to break the limitation of faster and lower energy consumption of all-optical switches, it is essential to introduce new physical principles. All-optical switches are one of the most important parts of integrated photonics. The traditional design method based on the micro-ring resonator, surface plasmon polaritons, photonic crystal, and metamaterial can still be continued, but the new physical concepts provide new design methods for the study of ultra-fast and ultra-low energy consumption all-optical switch. PT symmetry and exceptional points, topological insulators and bound states in the continuum are research hotspots in the field of photonics in recent years. On the one hand, people are looking for new physical phenomena, and on the other hand, they are also combining new physics with practical functional devices. The application of new physical effects provides new research ideas for the all-optical switch and broadens the design channel, which is expected to achieve ultra-compact, ultra-fast, and large-capacity all-optical information processing in the future.

Acknowledgements

This work was supported by the National Key Research and Development Program of China under Grant Nos. 2018YFB2200403 and 2018YFA0704404, and the National Natural Science Foundation of China under Grant Nos. 61775003, 11734001, 91950204, 11527901, and Beijing Municipal Science & Technology Commission No. Z191100007219001.

Data availability

The data that support the findings of this study are available from the corresponding author upon reasonable request.

[1] G. N. Dong, W. T. Deng, J. Hou, L. Chen, and X. L. Zhang, Opt Express **26**, 25630 (2018).
[2] T. Morioka and M. Saruwatari, Ieee J Sel Area Comm **6**, 1186 (1988).
[3] M. Jinno and T. Matsumoto, Ieee Photonic Tech L **2**, 349 (1990).
[4] M. Asobe, H. Itoh, T. Miyazawa, and T. Kanamori, Electron Lett **29**, 1966 (1993).
[5] T. Morioka and M. Saruwatari, Opt Eng **29**, 200 (1990).
[6] A. Hartsuiker, P. J. Harding, Y. R. Nowicki-Bringuier, J. M. Gerard, and W. L. Vos, J Appl Phys

104, 083105 (2008).
[7] H. Lu, X. M. Liu, L. R. Wang, Y. K. Gong, and D. Mao, Opt Express **19**, 2910 (2011).
[8] P. Colman, P. Lunnemann, Y. Yu, and J. Mork, Phys Rev Lett **117**, 233901 (2016).
[9] M. Forst, J. Niehusmann, T. Plotzing, J. Bolten, T. Wahlbrink, C. Moormann, and H. Kurz, Opt Lett **32**, 2046 (2007).
[10] M. Waldow, T. Plotzing, M. Gottheil, M. Forst, J. Bolten, T. Wahlbrink, and H. Kurz, Opt Express **16**, 7693 (2008).
[11] J. S. Pelc, K. Rivoire, S. Vo, C. Santori, D. A. Fattal, and R. G. Beausoleil, Opt Express **22**, 3797 (2014).
[12] M. Ono, M. Hata, M. Tsunekawa, K. Nozaki, H. Sumikura, H. Chiba, and M. Notomi, Nat Photonics **14**, 37 (2020).
[13] Z. J. Zhang, J. B. Yang, X. He, Y. X. Han, J. J. Zhang, J. Huang, D. B. Chen, and S. Y. Xu, Opt Commun **425**, 196 (2018).
[14] A. Karabchevsky, A. Hazan, and A. Dubavik, Adv Opt Mater **8**, 2000769 (2020).
[15] Z. Chai, X. Y. Hu, F. F. Wang, C. Li, Y. T. Ao, Y. Wu, K. B. Shi, H. Yang, and Q. H. Gong, Laser Photonics Rev **11**, 1700042 (2017).
[16] M. Takiguchi *et al.*, Acs Photonics **7**, 1016 (2020).
[17] M. Shoaei, M. K. Moravvej-Farshi, and L. Yousefi, J Opt Soc Am B **32**, 2358 (2015).
[18] C. M. Bender and S. Boettcher, Phys Rev Lett **80**, 5243 (1998).
[19] R. El-Ganainy, K. G. Makris, D. N. Christodoulides, and Z. H. Musslimani, Opt Lett **32**, 2632 (2007).
[20] K. G. Makris, R. El-Ganainy, D. N. Christodoulides, and Z. H. Musslimani, Phys Rev Lett **100**, 103904 (2008).
[21] Z. Y. Zhang, Y. Q. Zhang, J. T. Sheng, L. Yang, M. A. Miri, D. N. Christodoulides, B. He, Y. P. Zhang, and M. Xiao, Phys Rev Lett **117**, 123601 (2016).
[22] A. Guo, G. J. Salamo, D. Duchesne, R. Morandotti, M. Volatier-Ravat, V. Aimez, G. A. Siviloglou, and D. N. Christodoulides, Phys Rev Lett **103**, 093902 (2009).
[23] A. U. Hassan, B. Zhen, M. Soljacic, M. Khajavikhan, and D. N. Christodoulides, Phys Rev Lett **118**, 093002 (2017).
[24] X. L. Zhang, T. S. Jiang, and C. T. Chan, Light-Sci Appl **8, 1** (2019).
[25] A. Laha, D. Beniwal, S. Dey, A. Biswas, and S. Ghosh, Phys Rev A **101**, 063829 (2020).
[26] J. Doppler *et al.*, Nature **537**, 76 (2016).
[27] J. E. Moore, Nature **464**, 194 (2010).
[28] Y. Wu, X. Y. Hu, and Q. H. Gong, Phys Rev Mater **2**, 122201(R) (2018).
[29] R. L. Miao *et al.*, Nanoscale **11**, 14598 (2019).
[30] Y. C. Lin, S. H. Chou, and W. J. Hsueh, Opt Lett **45**, 4369 (2020).
[31] L. Fonda, Ann Phys-New York **22**, 123 (1963).
[32] H. Friedrich and D. Wintgen, Phys Rev A **31**, 3964 (1985).
[33] Q. J. Song, J. S. Hu, S. W. Dai, C. X. Zheng, D. Z. Han, J. Zi, Z. Q. Zhang, and C. T. Chan, Sci Adv **6**, 19 (2020).
[34] A. E. Miroshnichenko, S. Flach, and Y. S. Kivshar, Rev Mod Phys **82**, 2257 (2010).
[35] A. Tittl, A. Leitis, M. K. Liu, F. Yesilkoy, D. Y. Choi, D. N. Neshev, Y. S. Kivshar, and H. Altug, Science **360**, 1105 (2018).
[36] Y. C. Shuai, D. Y. Zhao, Z. B. Tian, J. H. Seo, D. V. Plant, Z. Q. Ma, S. H. Fan, and W. D. Zhou,

Opt Express **21**, 24582 (2013).
[37] N. Karl, P. P. Vabishchevich, S. Liu, M. B. Sinclair, G. A. Keeler, G. M. Peake, and I. Brener, Appl Phys Lett **115**, 141103 (2019).
[38] H. Z. Zhong, Z. Q. Liu, X. S. Liu, G. L. Fu, G. Q. Liu, J. Chen, and C. J. Tang, Opt Express **28**, 37294 (2020).
[39] Z. Han and Y. Cai, Opt Lett **46**, 524 (2021).